Introducing Hybrid Vehicle Dynamics in Microscopic Traffic Simulation

Yinglong He, Konstantinos Mattas, Michail A. Makridis, *Member, IEEE*, Dimitrios Komnos, Andres L. Marín, Georgios Fontaras, and Biagio Ciuffo

***Abstract*— Hybrid electric vehicles (HEVs) have reached the market share required to meaningfully affect many aspects of the road transport system, including traffic behaviour, energy consumption, and emissions. However, traffic models for hybrids remain insufficiently addressed in microscopic simulation because traditional models ignore vehicle dynamics, and therefore, cannot capture driving differences that exist among the hybrid, conventional, and electric vehicles. This study extends the lightweight microsimulation free-flow acceleration (MFC) model and fills the above gap in the literature by introducing hybrid vehicle dynamics into traffic simulation. First, the methodology underlying the MFC model to reproduce hybrid vehicle dynamics is described, for both charge depleting (CD) and charge sustaining (CS) modes. Then, the experimental setup for model validation and implementation was introduced. The simulations suggest the proposed MFC model can ensure smooth speed and acceleration profiles while converging to the steady state. The results show the MFC model can accurately capture the dynamics of the hybrid vehicle tested on the chassis dynamometer. The MFC model is compared with the Gipps' model and the intelligent driver model (IDM) regarding their abilities to reproduce driving trajectories of the hybrid vehicle. It was found, in CD mode, the MFC model leads to reductions in both speed and acceleration root mean square errors (RMSEs). In CS mode, the MFC model yields even greater accuracy gains. When predicting the 0-100 km/h acceleration specifications, the MFC model also outperforms the Gipps' and the IDM, reducing RMSE by 45.8 % and 51.9 %, respectively.**

***Index Terms*— Hybrid electric vehicles (HEVs), microscopic traffic simulation, driver behaviour, vehicle dynamics, charge depleting (CD), charge sustaining (CS).**

Manuscript received 24 January 2023; revised 28 September 2023; accepted 16 February 2024. This work was supported by the Joint Research Centre (JRC) of the European Commission. The Associate Editor for this article was D.-H. Lee. *(Corresponding author: Biagio Ciuffo.)*

Yinglong He is with the School of Mechanical Engineering Sciences, University of Surrey, GU2 7XH Guildford, U.K., and also with the School of the Physical Sciences, University of Cambridge, CB2 1TN Cambridge, U.K. (e-mail: ian.he@surrey.ac.uk).

Konstantinos Mattas, Dimitrios Komnos, Georgios Fontaras, and Biagio Ciuffo are with the Joint Research Centre (JRC), European Commission, 21027 Ispra, Italy (e-mail: Konstantinos.MATTAS@ec.europa.eu; Dimitrios.KOMNOS@ec.europa.eu; Georgios.FONTARAS@ec.europa.eu; Biagio.CIUFFO@ec.europa.eu).

Michail A. Makridis is with the Institute for Transport Planning and Systems (IVT), ETH Zürich, 8092 Zürich, Switzerland (e-mail: mmakridis@ethz.ch).

Andres L. Marín is with the Valencian Research Institute for Artificial Intelligence (VRAIN), Polytechnic University of Valencia, 46022 Valencia, Spain (e-mail: aflavmar@doctor.upv.es).

Digital Object Identifier 10.1109/TITS.2024.3378183

I. Introduction

MICROSCOPIC traffic simulation is an important tool widely used to enhance our understanding of various complex traffic-related phenomena. Although macroscopic and mesoscopic simulations have advantages like computational efficiency, they lack the necessary fidelity in many aspects such as actual traffic dynamics, road safety, energy or fuel consumption, emissions, etc. In addition, simulations with vehicles in the loop, or with detailed nano-level models can be cost-ineffective or even impossible to perform. Consequently, studies on connected and automated vehicles and relevant management systems are usually carried out through microscopic simulations [1], [2], [3], [4].

While microscopic simulation is an indispensable tool, it does not come without caveats. The number of different parts that have to be modelled such as the vehicle, the driver, the road geometry, the pavement conditions, and other simulation-specific parts, can be overwhelming. To carry out simulations, the modellers have to make assumptions and often use simplified models. One example is the impact of road geometry that is often not addressed, but recent experimental observations reveal that road geometry can even cause string instability under certain conditions [5]. Hence, developing modelling tools to take it into account is an active research topic [6], [7], [8]

One of the most challenging aspects to model is the behaviour of a driver/vehicle unit [9]. During the last decades, several car-following models and lane-changing models have been proposed [10], [11], [12]. For a more thorough investigation of the literature on this part, we suggest the following works [13], [14], [15]. However, the effectiveness of those models in reproducing the trajectories depends on the investigated quantity and the fidelity of the results [16], [17]. A significant disadvantage of widely used car-following models is the way the free flow acceleration is modelled, as shown by Ciuffo et al. [18]. Common car-following models focus on the distance maintaining behaviour and use simple equations for the acceleration part. Those simplifications can affect the estimation of energy consumption. Moreover, these models neglect vehicle dynamics in the acceleration process, and therefore, may withhold the emergence of dynamic traffic phenomena that can be only observable when using more advanced models with increased granularity [19].

This has led to an increase in research works regarding dynamics-based models, such as the Searle model [20], the

Rakha-Pasumarthy-Adjerid model [21], the Fadhloun-Rakha model [22], and the MFC free-flow model [23]. Such models ensure a more reliable and robust acceleration behaviour, by explicitly using vehicle dynamics in their formulations. The main focus of the present work is the MFC model, which can be coupled with existing car-following models, limiting the acceleration to what is realistic [24]. The model has been originally designed for internal combustion engine vehicles (ICEVs) in traffic simulation, and then has been extended to capture the dynamics of electric vehicles (EVs). A more detailed discussion of the main differences between the MFC and other dynamics-based models can be found in the work by He et al. [25]. Recently, the MFC model has been adopted by Aimsun, a commercial, widely-used microscopic traffic simulator [26]. Moreover, the MFC can be directly coupled with different tools, to have a more accurate fuel consumption estimation [24], [27]. Additionally, the current MFC version is openly available as a python library.[1]

A downside of the original MFC has been the inability to reproduce the dynamics of hybrid electric vehicles (HEVs) including full hybrids, mild hybrids, and plug-in hybrids, which are powered by an internal combustion engine (ICE) together with one or more electric motors (EMs). Their operation can be complicated, and harder to reproduce in simulation. There are detailed powertrain models that can simulate the operation of hybrid vehicles with high accuracy [28], but they are demanding in terms of computation time, making them impractical to be used for microscopic simulations. Moreover, such works are commonly backward looking, thus the velocity profile, and the respective accelerations are given as inputs.

In this work, we expand on the original MFC model formulation, to add the capability to simulate hybrid vehicles. In the MFC implementation for conventional vehicles [23], the engine full load potential was coupled with a detailed drivetrain model, including the clutch, the transmission, and the differential (or final drive). In the MFC implementation for electric vehicles [25], the electric motor full load power was coupled directly with the vehicle's final drive, for simulating the electric drivetrain with a fixed gear ratio. For the present study, a new model is developed, to capture the more realistic dynamics of hybrid vehicles. Moreover, the model is designed as an extension of the existing MFC implementation, making it possible for the dynamics of different vehicle types (ICE, EV and HEV) to be reproduced in microscopic simulation. Generally, HEVs can operate in two different modes: resembling an electric vehicle (charge depleting - CD); both the ICE and the electric motor being able to provide propulsion (charge sustaining - CS). The resulting MFC model has a flexible framework that can reproduce the operation of different electric and HEV configurations, with little sacrifice in the computational cost, suitable for microscopic simulations.

The proposed approach is validated against the trajectories of actual hybrid vehicles, tested on the laboratory chassis dynamometer. It should be noted that the new model, as the existing MFC implementation, takes over only the free-flow acceleration part, and for microscopic simulation experiment, it has to be coupled to an existing car-following model, regarding the control of the distance to downstream traffic. Additionally, it is compared against the free flow part of the Gipps' model [10], and that of the intelligent driver model (IDM) [29] using trajectory data. Finally, it is validated based on the official 0-100 km/h acceleration time from the hybrid vehicle specifications database.

Overall, the contributions of this work lie in the extension of the MFC model to include hybrid vehicle dynamics, providing valuable insights into the accurate representation of hybrid vehicles' behaviour in traffic simulations. The new model's capability to reproduce the operation of various powertrain configurations, with minimal computational cost, makes it a highly valuable tool for microscopic simulations. By addressing the specific driving differences among hybrid, conventional, and electric vehicles, our proposed MFC model offers a more comprehensive and reliable approach to enhancing the accuracy of traffic modelling in real-world scenarios.

II. MFC Model for Hybrid Vehicles

The MFC model proposed in this work is the first reported lightweight traffic model that can capture the dynamics of hybrid vehicles (including HEV and PHEV). Specifically, as shown in Figure 1 (a) and (b), this model derives the acceleration (a_n) of the hybrid vehicle n at a given speed (v_n) from three interacting components: the acceleration potential curve ($a_{n,ap}$), the deceleration potential curve ($a_{n,dp}$), and the driver behaviour function ($\beta_{n,d}$). The former two components (namely, $a_{n,ap}$ and $a_{n,dp}$) determine the propulsion and braking capabilities of a specific hybrid vehicle, respectively, based on its publicly available technical specifications and chassis dynamometer tests. The last component ($\beta_{n,d}$) describes the driver's response to traffic stimuli, e.g., the difference between the actual speed (v_n) and the desired speed (v_D, set by traffic control elements such as speed limits and traffic lights) in the free-flow acceleration regime and inter-vehicle distance in car-following acceleration regime. The $\beta_{n,d}$ is featured by two parameters including the driving style (DS) and the gear-shifting style (GS). The DS factor indicates the driving aggressiveness, namely, the percentage of the vehicle capabilities (i.e., $a_{n,ap}$ and $a_{n,dp}$) that drivers typically use. The GS factor determine the threshold speeds for gear shifting based on the habits of drivers.

In previous papers [23], [25], the study team developed MFC models for conventional internal combustion engine vehicles (ICEVs, including gasoline and diesel), battery electric vehicles (BEV), and series hybrid electric vehicles. As a follow-up study, this work proposes the MFC model for parallel hybrid electric vehicles, the system architecture and energy flows of which are illustrated in Figure 1 (c). Particularly, the electric motor (EM) is directly connected to the transmission input shaft. When the clutch is engaged, the internal combustion engine (ICE) and the EM can be coupled with each other, rotate at the same speed, and jointly deliver driving torque to the wheels [30]. The EM can also operate as a generator, which recovers the kinetic energy during braking or absorbs a portion of the engine power output, according

[1] https://github.com/JRCSTU/co2mpas_driver

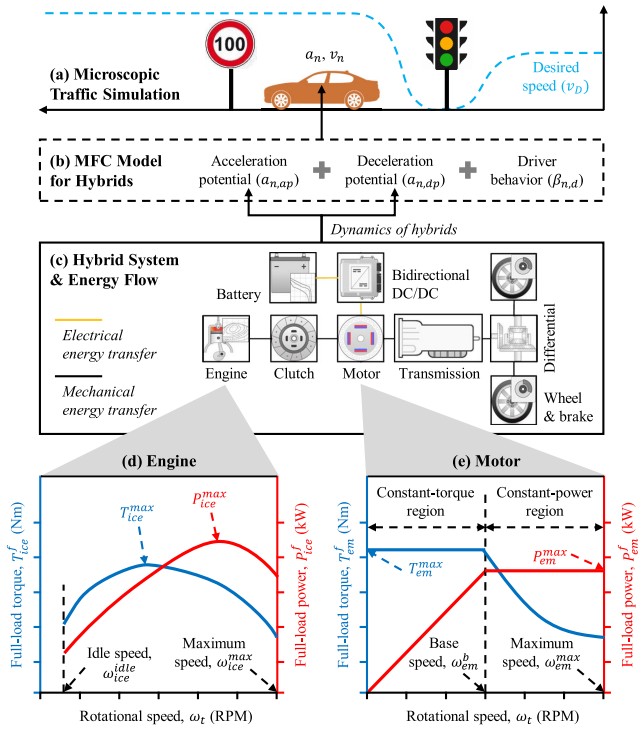

Fig. 1. Introducing the dynamics of hybrid vehicles into microsimulation. *Note:* DC = direct current; RPM = revolutions per minute.

to the battery state-of-charge (SoC) and the vehicle power demand [31], [32].

Therefore, the MFC model components, including $a_{n,ap}$, $a_{n,dp}$, and $\beta_{n,d}$, are sufficient to describe the dynamics of hybrid vehicles and the human factors as well as their interactions during driving. These components will be elaborated in next subsections.

A. Acceleration Potential Curve

To capture the maximum acceleration (i.e., the propulsion capability) across the entire speed range of the hybrid vehicle, the acceleration potential curve ($a_{n,ap}$) is given in Equation 1, which represents the interactions between the tractive and resistance forces acting on the wheels at a given speed.

$$a_{n,ap}(t) = \frac{F^f_T\big(v_n(t)\big) - F_R\big(v_n(t)\big)}{m}, \tag{1}$$

where $v_n(t)$ is the speed (m/s) of the hybrid vehicle n at a certain time (s) t; m is the vehicle operating mass (kg); F_R represents the resistance forces (N) including the aerodynamic drag, the rolling friction, and the grade resistance; F^f_T indicates the full-load tractive force (N) of the hybrid vehicle and can be expressed by Equation 2.

$$F^f_T(t) = \min\left(\frac{T^f_T\big(v_n(t)\big)}{r_w}, \mu \cdot m_{ta} \cdot g\right), \tag{2}$$

where r_w is the wheel radius (m); μ is the tire-road friction coefficient; m_{ta} is the vehicle mass on the tractive axle (kg); g is the gravitational acceleration (9.81 m/s^2); T^f_T is the full-load tractive torque (Nm), which varies with speed and hybrid mode (i.e., CD or CS) and can be described by Equation 3.

$$T^f_T(t) = \begin{cases} T^f_{em}\big(\omega_t(t)\big) \cdot i_t \cdot i_d \cdot \eta_d, & \text{for CD mode,} \\ \Big(T^f_{em}\big(\omega_t(t)\big) + T^f_{ice}\big(\omega_t(t)\big)\Big) \cdot i_t \cdot i_d \cdot \eta_d, & \text{for CS mode,} \end{cases} \tag{3}$$

$$\omega_t(t) = \frac{60 \cdot i_t \cdot i_d \cdot v_n(t)}{2\pi \cdot r_w}, \tag{4}$$

where T^f_{em} and T^f_{ice} are full load torques (Nm) of the electric motor (EM) and the internal combustion engine (ICE), respectively; i_t and i_d are the engaged gear ratios of the transmission and the differential, respectively; η_d is the driveline efficiency; ω_t is the rotational speed (RPM) of the transmission input shaft. Equation 3 reveals the distinction between charge sustaining (CS) and charge depleting (CD) modes within the MFC model during traffic flow simulation. When the vehicle operates in CS mode, both the internal combustion engine (ICE) and the electric motor (EM) work together to maintain the battery's charge level while providing propulsion. In contrast, when the vehicle is in CD mode, it functions exclusively in an all-electric mode, utilising the electric motor solely for propulsion. The relationship between ω_t and v_n is given by Equation 4.

Figure 1 (d) and (e) qualitatively explain the full-load speed-torque-power characteristics of the internal combustion engine (ICE) [23] and normal electric motor (EM) [33], [34], respectively. More specifically, the ICE full-load torque curve (T^f_{ice}) is low at idle speed (ω^{idle}_{ice}) and slowly ascends upwards before peaking (at T^{max}_{ice}) and dropping back down. Compared with T^f_{ice} curve, the ICE full-load power curve (P^f_{ice}) has a steeper slope with a larger peak speed. The full-load performance of the ICE can be described by Equation 5.

$$T^f_{ice}(t) = \frac{6 \times 10^4 \cdot P^f_{ice}\big(\omega_t(t)\big)}{2\pi \cdot \omega_t(t)}, \tag{5}$$

where P^f_{ice} is derived from the CO2MPAS generic ICE model [23], [35].

In contrast, Figure 1 (e) suggests that the EM provides the full-load torque and power curves that can be divided into two operation regions. First, in the lower speed region ($\omega_t < \omega^b_{em}$) or the constant-torque region, the full-load motor torque T^f_{em} is constant and equal to the motor's peak torque T^{max}_{em}; however, the full-load motor power P^f_{em} is directly proportional to the motor speed. Second, in the higher speed region or the constant-power region, P^f_{em} is constant and equal to the motor's peak power P^{max}_{em}, but T^f_{em} varies as a reciprocal function of the motor speed. Specifically, the motor's full-load torque T^f_{em} can be defined by Equation 6, which is a stepwise function of the EM's rotational speed ω_t.

$$T^f_{em}(t) = \begin{cases} T^{max}_{em}, & 0 \le \omega_t(t) < \omega^b_{em}, \\ \dfrac{6 \times 10^4 \cdot P^{max}_{em}}{2\pi \cdot \omega_t(t)}, & \omega^b_{em} \le \omega_t(t) < \omega^{max}_{em}, \end{cases} \tag{6}$$

$$\omega^b_{em} = \frac{6 \times 10^4 \cdot P^{max}_{em}}{2\pi \cdot T^{max}_{em}}, \tag{7}$$

where T^{max}_{em} and P^{max}_{em} are the peak torque (Nm) and the peak power (kW) of the EM, respectively; ω^{max}_{em} is the EM's

maximum rotational speed (RPM); ω_{em}^{b} is the EM's base speed (RPM) and can be calculated by Equation 7, which represents the split point between constant-torque and constant-power regions.

In addition, the aforementioned resistance force F_R as a function of speed and road grade is calculated by Equation 8.

$$F_R(t) = f_0 \cdot \cos\big(\theta(t)\big) + f_1 \cdot v_n(t) + f_2 \cdot v_n(t)^2 + mg \cdot \sin\big(\theta(t)\big), \quad (8)$$

where θ indicates the road grade (rad); f_0, f_1, and f_2 are road load coefficients (N, kg/s, and kg/m, respectively). More detailed explanations [36], [37] and typical values [38] of these coefficients can be found in the literature.

B. Deceleration Potential Curve

Based on prior experimental observations in the literatures [25] and [39], the deceleration potential ($a_{n,dp}$) of a typical passenger car can be formulated as a quadratic function of the driving speed (v_n), as shown in Equation 9.

$$\begin{cases} a_{n,dp}(t) = \epsilon\big(v_n(t)\big) \cdot a_d^{lim}, \\ a_d^{lim} = \mu \cdot g, \\ \epsilon(t) = b_0 + b_1 \cdot v_n(t) + b_2 \cdot v_n(t)^2, \end{cases} \quad (9)$$

where μ is the road friction coefficient; g is the gravitational acceleration (m/s^2); and thus a_d^{lim} is the vehicle's theoretical deceleration capability (assumed to be constant and equal to 4.80 m/s^2 in this study), which represents the maximum ability of the tire to sustain braking shear forces between the tire-road interface [22]; ϵ is the reduction factor that denotes the acceptable deceleration rate for drivers in the field, in which b_0, b_1, and b_2 are coefficients equal to -0.3924, -0.0563, 0.0012, respectively, based on the data from chassis dynamometer deceleration tests.

Equations 1-9 suggest that the acceleration potential ($a_{n,ap}$) and the deceleration potential ($a_{n,dp}$) are two vehicle-specific components in the MFC model. The former can be derived directly from the publicly available specifications. The latter is a generic component, namely, once its regression coefficients are estimated using the chassis dynamometer test data, they can be used for other vehicles of the same type (e.g., passenger cars).

C. Driver Behaviour Function

In the proposed MFC model, the driver behaviour function ($\beta_{n,d}$) can reproduce the patterns of drivers' acceleration, which serves as a variable reduction factor multiplied by $a_{n,ap}$ and $a_{n,dp}$ curves. Consequently, the typical acceleration and deceleration characteristics of drivers can be modelled in Equation 10.

$$a_n(t) = \begin{cases} \beta_{n,d}\big(v_n(t)\big) \cdot a_{n,ap}\big(v_n(t)\big), & 0 \le v_n(t) < v_D, \\ \beta_{n,d}\big(v_n(t)\big) \cdot a_{n,dp}\big(v_n(t)\big), & v_n(t) \ge v_D, \end{cases} \quad (10)$$

where a_n is the acceleration (m/s^2) of the hybrid vehicle n; v_D is the desired (or free-flow) speed (m/s); $\beta_{n,d}$ is the driving behaviour function, which is defined in Equation 11.

$$\beta_{n,d}(t) = DS \cdot \max\left[1 - \left(1 + \frac{c_0\big(v_n(t) - v_D\big)}{v_D + c_1}\right)^{c_2}, 1 - \left(1 - \frac{v_n(t) - v_D}{c_3}\right)^{c_4}\right], \quad (11)$$

where the factor DS denotes the driving style and ranges from 0 to 1; the coefficients c_0, c_1, c_2, c_3, and c_4 determine the way in which drivers approach the desired speed (v_D) and are set as 2, 0.1, 30, 50, and 100, respectively. The formulation and coefficients of Equation 11 have been derived from our previous MFC models, which were initially developed for conventional vehicles (see Equation 9 in [23]) and later extended to electric vehicles (see Equation 11 in [25]). In this study, we have undertaken further refinements and reorganisation of the formulation, resulting in a more simplified representation while preserving its inherent robustness and reliability.

Equations 1-11 show that the proposed MFC model, built on our well-established methodology [23], [25], efficiently captures the simple longitudinal dynamics of hybrid vehicles using $a_{n,ap}$ and $a_{n,dp}$, both of which are functions of the vehicle speed $v_n(t)$ and are parameterised using publicly available specifications at the start of the simulation. As a result, the model can be easily implemented and tested without introducing significant computational complexity. By relying on readily available technical specifications, the MFC model strikes a balance between accuracy and computational efficiency, making it well-suited for practical application in large-scale traffic simulations. In addition, the gear-shifting style (GS) in the driver model correlates the gear shift threshold points with the power curve of the vehicle and thus the powertrain operating speed. A dedicated driver gear-shifting model was developed by Makridis et al. [23] and adopted in this work.

III. Experimental Setup

The experimental setup describes chassis dynamometer tests performed in the premisses of the European Joint Research Centre (JRC), on-road driving tests, model calibration and validation against driving trajectories, validation against 0-100 km/h acceleration specifications, and two behavioural models (Gipps' and IDM) that are used in the validation workflow for comparison purposes.

A. Chassis Dynamometer Tests and On-Road Driving Tests

Chassis dynamometer tests were conducted at the Vehicle Emissions Laboratory (VELA) of the JRC, Ispra, aiming to validate the reliability of the acceleration and deceleration potential curves (i.e., $a_{n,ap}$ and $a_{n,dp}$). A 2016 Kia Niro PHEV was selected to conduct acceleration-deceleration test cycles in CD and CS modes. In the tests, the vehicle was operated within a speed range between 0 and 35 m/s. The testbed can collect data with a 10 Hz measurement rate.

On-road driving tests were performed between December 2021 and March 2023 using a Volkswagen Golf 8 PHEV in both CD and CS modes, covering diverse traffic environments including rural, urban, and motorway, where the vehicle operated at average speeds of 68.9 km/h, 31.5 km/h, and 107.8 km/h, respectively. We collected real-world operational data to calibrate and validate the models. The test routes included various uphill and downhill sections, providing an

TABLE I
MAIN SPECIFICATIONS OF THE TEST HYBRID VEHICLES

Specifications	Symbols	Units	Kia Niro	VW Golf 8
Operating mass	m	kg	1421	1698
Height	H	m	1.55	1.48
Width	W	m	1.81	1.79
Wheel radius	r_w	m	0.33	0.33
Transmission gear ratios	i_t	na	[3.87, 2.22, 1.37, 0.96, 0.93, 0.77]	[13.13, 8.0, 5.34, 3.83, 2.95, 2.42]
Differential gear ratio	i_d	na	3.23	1.00
0-100 km/h acceleration time	$T_{0-100km/h}$	s	11.5	7.4
Top speed	v_{lim}	km/h	162	220
Battery capacity	C_{bat}	kWh	1.56	13.0
EM's peak torque	T_{em}^{max}	Nm	44.5	330
EM's peak power	P_{em}^{max}	kW	170	70
ICE's peak torque	T_{ice}^{max}	Nm	147	250
ICE's peak power	P_{ice}^{max}	kW	77	110

Note: na = not applicable.

ideal setting for evaluating different tractive load conditions. To determine the road gradient, we extracted the elevation profile using the GPS Visualizer (www.gpsvisualizer.com). Table I lists the main specifications for the hybrid vehicles being examined above.

B. Calibration and Validation Experiments Against Trajectory Data

The hybrid vehicle's CD and CS driving trajectories were employed to calibrate and validate the parameters of the proposed model. The LMFIT (non-linear least-squares minimization and curve-fitting) served as the optimization tool. According to the approaches in the literature [40], the calibration objective function is defined based on the sums of squared errors, as described below.

$$J(\chi) = \sum_{i=1}^{K} \left(\ln \left(\frac{v_\chi(i)}{v_N(i)} \right) \right)^2, \forall \chi, \tag{12}$$

where i is a distance instance (every 2 m along the predefined path); v_N is the measured speed of the naturalistic driving trajectory; v_χ is the speed trajectory produced by the model with a vector of parameters χ.

Apart from the proposed MFC model (for hybrids), another two widely accepted behaviour models, namely, Gipps' and IDM, are utilized for comparison purposes in the calibration and validation experiments. The free-flow term of the Gipps' model is described below.

$$a_n(t) = \max \left(\alpha \cdot a_0 \cdot \left(1 - \frac{v_n(t)}{v_D} \right) \cdot \left(\lambda + \frac{v_n(t)}{v_D} \right)^\gamma, b_0 \right), \tag{13}$$

$$\alpha = \frac{(1+\gamma)^{1+\gamma}}{\gamma^\gamma \cdot (1+\lambda)^{1+\gamma}}, \tag{14}$$

where v_n and a_n are simulated speed (m/s) and acceleration (m/s^2) at time t (s); v_D is the desired speed (m/s); a_0 is the desired acceleration (m/s^2); and b_0 indicates the most severe braking that the driver wishes to undertake and is equal to -3 m/s^2 in this work. The coefficients α, λ, and γ are assumed to be 2.5, 0.025, and 0.5 in the original formulation of the Gipps' model [10], but for the sake of generality, they are specified as adjustable parameters to fit different driving behaviour. Moreover, Ciuffo et al. [41] reported that α, λ, and γ follow the relationship described in Equation 14. In terms of the IDM, according to previous studies [42], its free-flow branch can be expressed as Equation 15.

$$a_n(t) = \max \left(a_0 \cdot \left(1 - \frac{v_n(t)}{v_D} \right)^\delta, b_0 \right), \tag{15}$$

where δ is an exponent factor, which controls the decrease in acceleration when desired velocity is met by the driver [43].

Table II summarizes the three free-flow acceleration models, namely, the Gipps', the IDM, and the proposed MFC. As described by their equations, these models have the same output (a_n) and input (v_n and v_D) variables. To construct calibration experiments, the calibration parameters and the corresponding constraints of these models are provided. Since the MFC is a dynamics-based model, the vehicle-related parameters in the equations can be derived from technical specifications or empirical data.

TABLE II
CALIBRATION PARAMETERS AND THEIR CONSTRAINTS

Model	Equation(s)	Parameters
Gipps'	(13)-(14)	$a_0 \in [0.5, 4], \lambda \in [0.001, 5], \gamma \in [0.5, 4]$
IDM	(15)	$a_0 \in [0.5, 4], \delta \in [0.1, 4]$
MFC	(1)-(11)	$DS \in [0.1, 1], GS \in [0.1, 1]$

Note: IDM = intelligent driver model; MFC = microsimulation free-flow acceleration model.

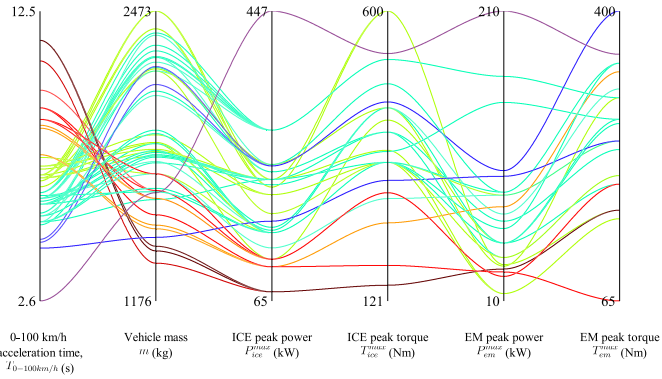

Fig. 2. Main specifications of hybrid vehicles from the database. *Note:* ICE = internal combustion engine; EM = electric motor.

C. Validation Against 0–100 Km/h Acceleration Specifications

The publicly available vehicle specifications often provide 0-100 km/h acceleration time ($T_{0-100km/h}$, s), which denotes vehicle's acceleration capability in real-world driving tests, and therefore, can be utilized to validate the model's ability to capture hybrid vehicles' acceleration performances. To this end, a hybrid vehicle specification database was created. Figure 2 shows the main specifications of 203 hybrid vehicles, which are associated with their acceleration performances and include the vehicle mass, and the power and the torque of the ICE and the EM. The data in this parallel plot suggest that

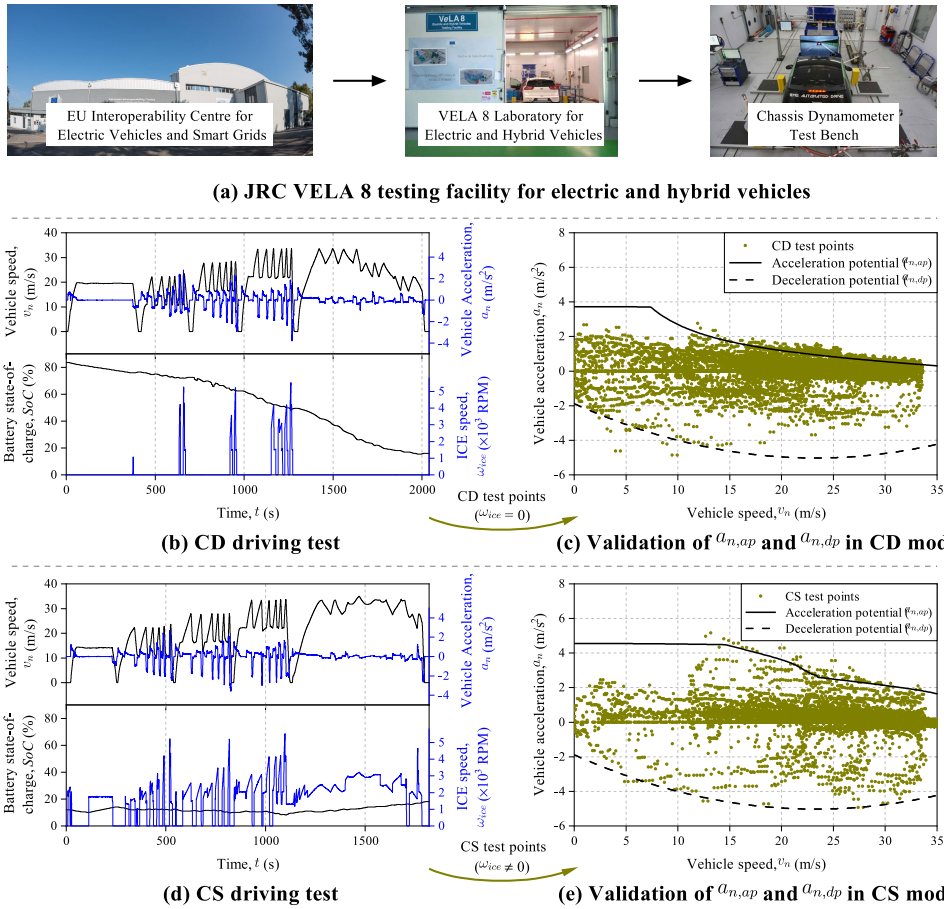

Fig. 3. Chassis dynamometer tests of a hybrid vehicle to validate $a_{n,ap}$ and $a_{n,dp}$ curves. *Note:* EU = European Union; JRC = Joint Research Centre; VeLA = Vehicle Electric Laboratory; CD = charge depleting; CS = charge sustaining; ICE = internal combustion engine; SoC = state-of-charge; RPM = revolutions per minute.

higher performances of the EM and the ICE (i.e., P_{em}^{max}, T_{em}^{max}, P_{ice}^{max}, T_{ice}^{max}) can lead to lower 0-100 km/h acceleration time ($T_{0-100km/h}$), which ranges from 2.6 to 11.5 s.

IV. Results and Discussion

This section gives a comprehensive analysis regarding the results obtained from the experimental and simulation tests described above.

A. Model Validation Using the Laboratory Data

As elaborated in Figure 1, the acceleration potential ($a_{n,ap}$) and the deceleration potential ($a_{n,dp}$) are two key components in the proposed MFC model. To demonstrate their capabilities to reproduce the longitudinal driving dynamics of the hybrid vehicles, Figure 3 validates the theoretical $a_{n,ap}$ and $a_{n,dp}$ curves from the MFC model against the experimental data from the chassis dynamometer tests in the laboratory. Figure 3 (a) illustrates the EU Interoperability Centre at the JRC (Ispra) and the chassis dynamometer test bench for hybrid vehicles.

Figure 3 (b) and (d) present the driving data collected from the hybrid vehicle on the chassis dynamometer in CD and CS modes, respectively. More specifically, their top subplot gives the vehicle speed (m/s) and acceleration (m/s^2); while the bottom one shows the battery state-of-charge (SoC, %) and the rotational speed (RPM) of the ICE. The initial values of the battery SoC in CD and CS modes are 83.5% and 12%, respectively. Figure 3 (b) suggests that CD mode aims to exhaust the all-electric range (AER), and therefore, prioritizes the use of the EM over the ICE. The ICE only operates if the vehicle's power demand exceeds the limits of the EM. The proposed MFC model assumes that hybrid vehicles in CD mode are propelled by the EM only for simplification purposes, as described by Equation 3. Therefore, Figure 3 (c) selects the CD test points, where the ICE speed is equal to zero ($\omega_{ice} = 0$). In contrast, as demonstrated in Figure 3 (d), the CS mode, to which the hybrid vehicle switches after the battery has reached the minimum SoC threshold, uses a combination of ICE and EM management to maintain the battery SoC at a specified level and at the same time meet the vehicle's power demand. Consequently, Figure 3 (e) chooses the CS test points where $\omega_{ice} \neq 0$ to validate this combined propulsion capability. The results suggest that the theoretical $a_{n,ap}$ curve, which derived directly from hybrid vehicle specifications, demonstrates a fair correlation with the upper boundary test points. Furthermore, the empirical $a_{n,dp}$ curve is very close to the lower boundary test points. In addition, by comparing Figure 3 (c) and (e), both the empirical data points and theoretical $a_{n,ap}$ curves suggest that the CD mode has much lower acceleration capability at high speeds compared with the CS mode.

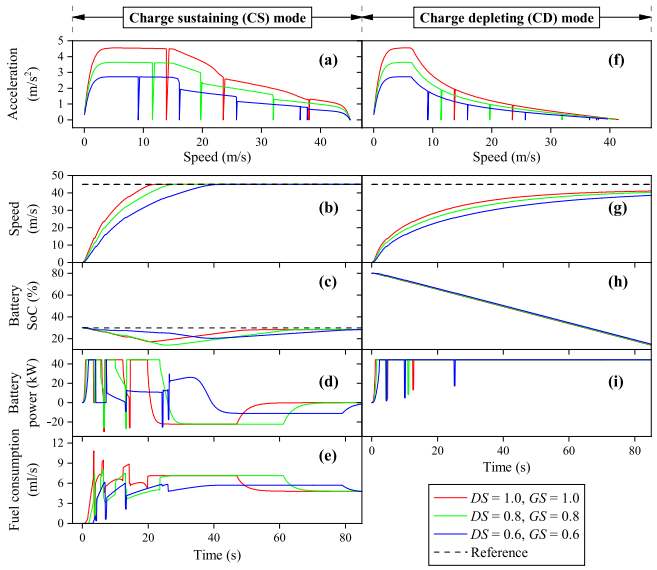

Fig. 4. Acceleration simulation of the MFC model with different driving and gear-shifting styles (represented by DS and GS, respectively): (a)-(e) CS mode; (f)-(i) CD mode. *Note:* DS = driving style; GS = gear-shifting style; SoC = state-of-charge.

B. Model Implementation in Microsimulation

Figures 4 and 5 show the modelling results after implementing the developed MFC model in microsimulation. The colour-coded solid lines depict the profiles of three indicative drivers for the same hybrid vehicle. Specifically, the first driver, $(DS, GS) = (1, 1)$, is the most aggressive, as the full capabilities of the hybrid's acceleration and deceleration are exploited. The second driver, $(DS, GS) = (0.8, 0.8)$, is more timid and the third, $(DS, GS) = (0.6, 0.6)$, is the most conservative.

Figure 4 presents the driving data of different drivers and compares the CD and the CS modes in acceleration simulation, where a wide speed range (from 0 to 45 m/s) is selected to comprehensively demonstrate the model performance and the differences between drivers. The speed-acceleration profiles of Figure 4 (a) and (f) indicate that the smaller the GS, the earlier the driver changes gears, that is in line with previous observations in the literature [23]. Figure 4 (b)-(e) and (g)-(i) are time-series data of the CS and CD modes, respectively. Specifically, the time-speed profiles suggest that, in CS mode, the hybrid vehicle can reach the reference speed (i.e., 45 m/s) within 40 s. In CD mode, however, it cannot reach the reference speed even after a long period due to limited power derived from the EM only. In addition, Figure 4 (c) and (h) show the battery SoC, in which the CS mode manages to maintain the battery SoC at 30 % by coordinating the power outputs of the ICE and the EM; while the CD mode deplete the battery SoC from 80 % to 20 %. In Figure 4 (e), the fuel consumption (ml/s) results imply that the aggressive driver, $(DS, GS) = (1, 1)$, consumes more fuel.

Figure 5 provides the speed and acceleration results of the proposed MFC model in a driving scenario with varying road speed limits. It is clear that, in both CS and CD modes, the MFC model can guarantee a smooth transition between different speed levels; while obvious oscillations or overshoots can be avoided when gradually approaching the reference speed. This smooth feature is praiseworthy given that significant and omnipresent acceleration cliffs are observed in many renowned traffic models [22].

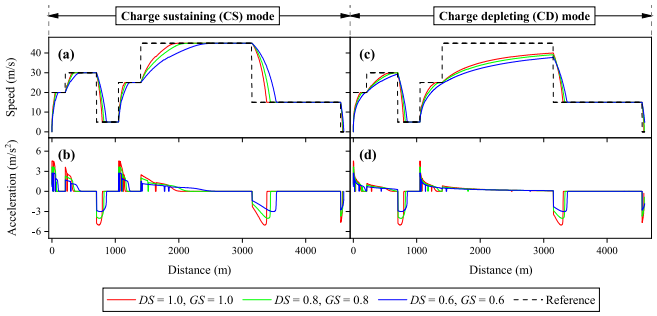

Fig. 5. Artificial driving cycle with the response of the MFC model: (a)-(b) CS mode; (c)-(d) CD mode.

TABLE III

ROOT MEAN SQUARE ERRORS (RMSES) OF SPEED (v_n) AND ACCELERATION (a_n) WHEN CALIBRATING AND VALIDATING MODELS AGAINST DRIVING TRAJECTORIES OF HYBRID VEHICLES

		Kia Niro		VW Golf 8	
		CD	CS	CD	CS
Calibration					
v_n (m/s)	MFC	0.30	0.26	0.23	0.13
	Gipps	0.51	0.77	0.37	0.31
	IDM	0.78	1.15	0.55	0.47
a_n m^2/s	MFC	0.12	0.12	0.21	0.09
	Gipps	0.17	0.33	0.22	0.12
	IDM	0.25	0.46	0.28	0.16
Validation					
v_n (m/s)	MFC	0.15	0.05	0.20	0.75
	Gipps	0.18	0.17	0.31	0.88
	IDM	0.29	0.27	0.45	2.68
a_n m^2/s	MFC	0.04	0.02	0.20	0.18
	Gipps	0.05	0.05	0.24	0.23
	IDM	0.06	0.07	0.30	0.34

Note: IDM = intelligent driver model; MFC = microsimulation free-flow acceleration model; CD = charge depleting; CS = charge sustaining.

C. Calibration and Validation Against Driving Trajectories

Table III presents the root mean square errors (RMSEs) for speed (v_n) and acceleration (a_n) during the calibration and validation of models using driving trajectories from hybrid vehicles. The table is divided into two sections: calibration (upper) and validation (lower). It includes results for two different vehicles, Kia Niro and VW Golf 8, operating in two hybrid modes: CD (charge depleting) and CS (charge sustaining). As described in Section III, Kia Niro underwent in-lab driving tests on a chassis dynamometer, whereas VW Golf 8 was subjected to on-road driving tests that encompassed diverse traffic conditions and varying road gradients.

Regarding speed (v_n) calibration, the MFC model demonstrated noteworthy precision. For the Kia Niro, the MFC achieved RMSE values of 0.30 m/s in CD mode and 0.26 m/s in CS mode. Similarly, when applied to the VW Golf 8, the MFC yielded RMSE values of 0.23 m/s in CD mode and 0.13 m/s in CS mode. It's worth highlighting that, during this calibration phase, both the Gipps' model and the IDM produced RMSE values that exceeded those of the MFC.

In terms of acceleration (a_n) calibration, the MFC model delivered exceptional results. It recorded RMSEs of 0.12 m^2/s

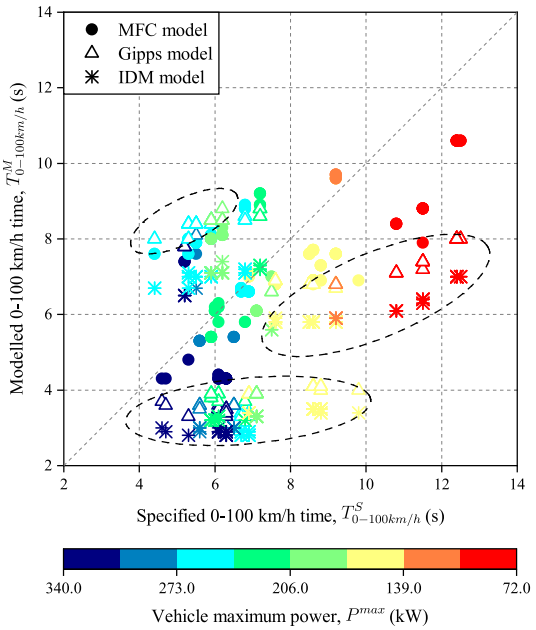

Fig. 6. Validation of the 0-100 km/h acceleration time predicted by models against the official specifications of hybrid vehicles.

for both CD and CS modes of the Kia Niro. For the VW Golf 8, the MFC demonstrated an RMSE of 0.21 m^2/s in CD mode and a notably lower 0.09 m^2/s in CS mode. Once again, the MFC model outperformed its counterparts, the Gipps' model and IDM.

In the validation phase, the MFC model maintained its superior performance. It delivered competitive RMSE values for speed (v_n), with 0.15 m/s for the Kia Niro in CD mode, 0.05 m/s in CS mode, 0.20 m/s for the VW Golf 8 in CD mode, and 0.75 m/s in CS mode. These values surpassed the performance of the Gipps' model and IDM. In acceleration (a_n) validation, the MFC model demonstrated its superiority with RMSEs of 0.04 m^2/s for the Kia Niro in CD mode, 0.02 m^2/s in CS mode, 0.20 m^2/s for the VW Golf 8 in CD mode, and 0.18 m^2/s in CS mode, reaffirming its consistent excellence across diverse vehicle types and driving conditions.

In summary, the MFC model outperformed the Gipps' model and IDM, delivering lower RMSE values in both calibration and validation phases for v_n and a_n prediction.

D. Validation Against 0-100 Km/h Acceleration Specifications

As illustrated in Figure 6, the models are validated using official 0-100 km/h acceleration time ($T_{0-100km/h}$) based on the specifications database of 203 hybrid vehicles, which is described in Figure 2. Specifically, the scatter plot in Figure 6 compares the acceleration time predicted by models (i.e., $T^M_{0-100km/h}$) with the value in technical specifications of the corresponding hybrid vehicle (i.e., $T^S_{0-100km/h}$). In addition, the varying marker color depends on the vehicle maximum power (P^{max}, a combined power delivered from the EM and the ICE). The results in this graph suggest that, compared to the Gipps' model and the IDM, the MFC model leads to a cluster more closely located around the diagonal, indicating small errors between the predicted ($T^M_{0-100km/h}$) and specified ($T^S_{0-100km/h}$) values. In contrast, as circled by the black dash lines, the Gipps' model and the IDM both significantly underestimate $T_{0-100km/h}$ values (see circled clusters below the diagonal). In addition, Gipps' model gives rise to overestimated predictions when P^{max} approximately ranges between 200 and 270 kW.

TABLE IV
RMSE BETWEEN THE PREDICTED ($T^M_{0-100km/h}$) AND THE SPECIFIED ($T^S_{0-100km/h}$) 0-100 KM/H ACCELERATION TIME

Model	RMSE (s)	Reduction (%, relative to MFC)
MFC	1.65	na
Gipps'	3.05	45.8
IDM	3.44	51.9

Note: RMSE = root mean square error; IDM = intelligent driver model; MFC = microsimulation free-flow acceleration model; na = not applicable.

Table IV summarizes the data in Figure 6 and gives the RMSE between the predicted ($T^M_{0-100km/h}$) and specified ($T^S_{0-100km/h}$) 0-100 km/h acceleration time. The results show that the Gipps' model and the IDM yield $T_{0-100km/h}$ RMSEs of 3.05 and 3.44 s, respectively. Alternatively, the proposed MFC model can deliver a much more accurate $T_{0-100km/h}$ prediction with a RMSE of 1.65 s, which is 45.8 % and 51.9 % lower than those of the Gipps' model and the IDM, respectively.

V. CONCLUSION

The present work builds on the MFC modelling framework and proposes the first traffic model that can capture the dynamics of hybrid electric vehicles, which differ from conventional and electric ones in driving capabilities/behaviours due to different propulsion systems and dynamics. The MFC model developed in this study is a lightweight and robust approach to reproducing the dynamics of hybrids in traffic simulation, especially the hybrids' speed and torque coupling between the internal combustion engine (ICE) and the electric motor (EM) charge depleting (CD) and charge sustaining (CS) modes. The results suggest that:

- The data from chassis dynamometer tests of the hybrid vehicle are well-approximated by the acceleration and deceleration potential curves underlying the proposed MFC model.
- After being implemented in microsimulation, the MFC model can ensure smooth transitions between different speed levels, avoiding oscillations or overshoots.
- When reproducing driving trajectories of the hybrid vehicle, in CD mode, the MFC model can yield significant reductions in root mean square errors (RMSEs) of both speed and acceleration, compared with the Gipps' model (by ∼16 %) and the intelligent driver model (IDM, by ∼40 %). In CS mode, the MFC model can give rise to even greater accuracy gains due to its accurate representation of ICE-EM coupling dynamics.
- The MFC model also outperforms traditional models in predicting the 0-100 km/h acceleration specifications. Its prediction RMSE is 45.8 % and 51.9 % lower than those of the Gipps' model and the IDM, respectively.

This study successfully demonstrates the capability of the MFC model to capture hybrid vehicle dynamics, however, there are several important aspects that require further investigation to enhance the applicability and scope of our findings:

- The performance of the MFC model in simulating a broader spectrum of hybrid vehicle configurations (e.g., power-split) remains unexplored within the current study. This will provide a deeper understanding of the model's performance and its adaptability to different hybrid vehicle designs.
- The potential ramifications of hybrid vehicle adoption on traffic patterns, energy consumption, and emissions were not delved into in this study, limiting the broader applicability of our findings. This analysis will contribute to a more holistic understanding of the impact of hybrid vehicle integration in transportation networks.

ACKNOWLEDGMENT

The opinions expressed in this manuscript are those of the authors and should not be considered to represent an official opinion of the European Commission. The authors are grateful to Alessandro Tansini and the JRC Vehicle Emissions Laboratory (VELA) team for their support during the experiments and validations.

REFERENCES

[1] S. E. Shladover, D. Su, and X.-Y. Lu, "Impacts of cooperative adaptive cruise control on freeway traffic flow," *Transp. Res. Rec.*, vol. 2324, no. 1, pp. 63–70, 2012.

[2] B. van Arem, C. J. G. van Driel, and R. Visser, "The impact of cooperative adaptive cruise control on traffic-flow characteristics," *IEEE Trans. Intell. Transp. Syst.*, vol. 7, no. 4, pp. 429–436, Dec. 2006.

[3] A. Kesting, M. Treiber, M. Schönhof, and D. Helbing, "Extending adaptive cruise control to adaptive driving strategies," *Transp. Res. Rec.*, vol. 2000, no. 1, pp. 16–24, Jan. 2007.

[4] K. Mattas et al., "Simulating deployment of connectivity and automation on the Antwerp ring road," *IET Intell. Transp. Syst.*, vol. 12, no. 9, pp. 1036–1044, 2018.

[5] B. Ciuffo et al., "Requiem on the positive effects of commercial adaptive cruise control on motorway traffic and recommendations for future automated driving systems," *Transp. Res. C, Emerg. Technol.*, vol. 130, Sep. 2021, Art. no. 103305.

[6] Y. He, K. Mattas, R. Dona, G. Albano, and B. Ciuffo, "Introducing the effects of road geometry into microscopic traffic models for automated vehicles," *IEEE Trans. Intell. Transp. Syst.*, vol. 23, no. 8, pp. 13604–13613, Aug. 2022.

[7] B. Goñi Ros, V. L. Knoop, Y. Shiomi, T. Takahashi, B. van Arem, and S. P. Hoogendoorn, "Modeling traffic at sags," *Int. J. Intell. Transp. Syst. Res.*, vol. 14, no. 1, pp. 64–74, Jan. 2016.

[8] B. Goñi-Ros et al., "Using advanced adaptive cruise control systems to reduce congestion at sags: An evaluation based on microscopic traffic simulation," *Transp. Res. C, Emerg. Technol.*, vol. 102, pp. 411–426, May 2019.

[9] M. Makridis, A. Anesiadou, K. Mattas, G. Fontaras, and B. Ciuffo, "Characterizing driver heterogeneity within stochastic traffic simulation," *Transportmetrica B-Transp. Dyn.*, vol. 11, no. 1, pp. 725–743, 2023.

[10] P. G. Gipps, "A behavioural car-following model for computer simulation," *Transp. Res. B, Methodol.*, vol. 15, no. 2, pp. 105–111, 1981.

[11] A. Kesting, M. Treiber, and D. Helbing, "Enhanced intelligent driver model to access the impact of driving strategies on traffic capacity," *Philosoph. Trans. Roy. Soc. A*, vol. 368, no. 1928, pp. 4585–4605, Oct. 2010.

[12] G. F. Newell, "A simplified car-following theory: A lower order model," *Transp. Res. B, Methodol.*, vol. 36, no. 3, pp. 195–205, Mar. 2002.

[13] B. Cao and Z. Yang, "Car-following models study progress," in *Proc. 2nd Int. Symp. Knowl. Acquisition Model.*, vol. 3, Nov. 2009, pp. 190–193.

[14] D. Helbing, "Traffic and related self-driven many-particle systems," *Rev. Modern Phys.*, vol. 73, no. 4, pp. 1067–1141, Dec. 2001.

[15] M. Brackstone and M. McDonald, "Car-following: A historical review," *Transp. Res. F, Traffic Psychol. Behaviour*, vol. 2, no. 4, pp. 181–196, Dec. 1999.

[16] V. Punzo, Z. Zheng, and M. Montanino, "About calibration of car-following dynamics of automated and human-driven vehicles: Methodology, guidelines and codes," *Transp. Res. C, Emerg. Technol.*, vol. 128, Jul. 2021, Art. no. 103165.

[17] Y. He, M. Montanino, K. Mattas, V. Punzo, and B. Ciuffo, "Physics-augmented models to simulate commercial adaptive cruise control (ACC) systems," *Transp. Res. C, Emerg. Technol.*, vol. 139, Jun. 2022, Art. no. 103692.

[18] B. Ciuffo, M. Makridis, T. Toledo, and G. Fontaras, "Capability of current car-following models to reproduce vehicle free-flow acceleration dynamics," *IEEE Trans. Intell. Transp. Syst.*, vol. 19, no. 11, pp. 3594–3603, Nov. 2018.

[19] M. Makridis, L. Leclercq, B. Ciuffo, G. Fontaras, and K. Mattas, "Formalizing the heterogeneity of the vehicle-driver system to reproduce traffic oscillations," *Transp. Res. C, Emerg. Technol.*, vol. 120, Nov. 2020, Art. no. 102803.

[20] J. Searle, "Equations for speed, time and distance for vehicles under maximum acceleration," SAE, Tech. Paper 1999-01-00 78, 1999, doi: 10.4271/1999-01-0078.

[21] H. Rakha, "Validation of van Aerde's simplified steadystate car-following and traffic stream model," *Transp. Lett.*, vol. 1, no. 3, pp. 227–244, Jul. 2009.

[22] K. Fadhloun and H. Rakha, "A novel vehicle dynamics and human behavior car-following model: Model development and preliminary testing," *Int. J. Transp. Sci. Technol.*, vol. 9, no. 1, pp. 14–28, Mar. 2020.

[23] M. Makridis, G. Fontaras, B. Ciuffo, and K. Mattas, "MFC free-flow model: Introducing vehicle dynamics in microsimulation," *Transp. Res. Rec.*, vol. 2673, no. 4, pp. 762–777, Apr. 2019.

[24] M. Makridis, K. Mattas, C. Mogno, B. Ciuffo, and G. Fontaras, "The impact of automation and connectivity on traffic flow and CO_2 emissions. A detailed microsimulation study," *Atmos. Environ.*, vol. 226, Apr. 2020, Art. no. 117399.

[25] Y. He, M. Makridis, K. Mattas, G. Fontaras, B. Ciuffo, and H. Xu, "Introducing electrified vehicle dynamics in traffic simulation," *Transp. Res. Rec.*, vol. 2674, no. 9, pp. 776–791, Jul. 2020.

[26] (2022). *MFC and Battery Consumption Model—Aimsun*. [Online]. Available: https://www.aimsun.com/knowledge-base/mfc-and-battery-consumption-model/

[27] C. Mogno et al., "The application of the CO_2MPAS model for vehicle CO_2 emissions estimation over real traffic conditions," *Transp. Policy*, vol. 124, pp. 152–159, Aug. 2022.

[28] A. Tansini, "Flexible calculation approaches to support the European CO_2 emissions regulatory scheme for road vehicles," Ph.D. dissertation, Energy Dept., Politecnico di Torino, Torino, 2020.

[29] M. Treiber, A. Hennecke, and D. Helbing, "Congested traffic states in empirical observations and microscopic simulations," *Phys. Rev. E, Stat. Phys. Plasmas Fluids Relat. Interdiscip. Top.*, vol. 62, no. 2, p. 1805, 2000.

[30] C. Mi and M. A. Masrur, *Hybrid Electric Vehicles: Principles and Applications With Practical Perspectives*. Hoboken, NJ, USA: Wiley, 2017.

[31] Y. He et al., "Multiobjective component sizing of a hybrid ethanol-electric vehicle propulsion system," *Appl. Energy*, vol. 266, May 2020, Art. no. 114843.

[32] Y. He et al., "Multiobjective co-optimization of cooperative adaptive cruise control and energy management strategy for PHEVs," *IEEE Trans. Transport. Electrific.*, vol. 6, no. 1, pp. 346–355, Mar. 2020.

[33] Z. Tian, C. Zhang, and S. Zhang, "Analytical calculation of magnetic field distribution and stator iron losses for surface-mounted permanent magnet synchronous machines," *Energies*, vol. 10, no. 3, p. 320, Mar. 2017.

[34] B. Bilgin et al., "Making the case for electrified transportation," *IEEE Trans. Transport. Electrific.*, vol. 1, no. 1, pp. 4–17, Jun. 2015.

[35] S. Tsiakmakis et al., "Introducing a new emissions certification procedure for European light-duty vehicles: Monte Carlo simulation of the potential effect on fleet carbon dioxide emissions," *Transp. Res. Rec., J. Transp. Res. Board*, vol. 2572, no. 1, pp. 66–77, Jan. 2016.

[36] S. Tsiakmakis, G. Fontaras, B. Ciuffo, and Z. Samaras, "A simulation-based methodology for quantifying European passenger car fleet CO_2 emissions," *Appl. Energy*, vol. 199, pp. 447–465, Aug. 2017.

[37] Y. He, M. Makridis, G. Fontaras, K. Mattas, H. Xu, and B. Ciuffo, "The energy impact of adaptive cruise control in real-world highway multiple-car-following scenarios," *Eur. Transp. Res. Rev.*, vol. 12, no. 1, pp. 1–11, Dec. 2020.

[38] L. Küng, T. Bütler, G. Georges, and K. Boulouchos, "How much energy does a car need on the road?" *Appl. Energy*, vol. 256, Dec. 2019, Art. no. 113948.

[39] A. K. Maurya and P. S. Bokare, "Study of deceleration behaviour of different vehicle types," *Int. J. raffic Transp. Eng.*, vol. 2, no. 3, pp. 253–270, Sep. 2012.

[40] M. Treiber and A. Kesting, "Microscopic calibration and validation of car-following models—A systematic approach," *Proc.-Social Behav. Sci.*, vol. 80, pp. 922–939, Jun. 2013.

[41] B. Ciuffo, V. Punzo, and M. Montanino, "Thirty years of Gipps' car-following model: Applications, developments, and new features," *Transp. Res. Rec.*, vol. 2315, no. 1, pp. 89–99, Jan. 2012.

[42] W. J. Schakel, B. Van Arem, and B. D. Netten, "Effects of cooperative adaptive cruise control on traffic flow stability," in *Proc. 13th Int. IEEE Conf. Intell. Transp. Syst.*, Sep. 2010, pp. 759–764.

[43] H. Tanveer, M. M. Mubasher, and S. W. Jaffry, "Integrating human panic factor in intelligent driver model," in *Proc. 3rd Int. Conf. Advancements Comput. Sci. (ICACS)*, Feb. 2020, pp. 1–6.

Yinglong He received the B.E. and M.Sc. degrees in energy and power engineering from Huazhong University of Science and Technology (HUST), Wuhan, China, in 2014 and 2017, respectively, and the Ph.D. degree in mechanical engineering from the University of Birmingham (UoB), U.K., in 2021.

He was a Post-Doctoral Research Associate (PDRA) with the Institute of Astronomy (IoA), University of Cambridge. He held an expert position with the Directorate for Energy, Transport, and Climate, Joint Research Centre (JRC), European Commission. He is currently a Lecturer in resilient transport systems, electric vehicles, and autonomous systems. His research has enabled Aimsun Next, a mobility modeling software owned by Siemens, to achieve more accurate fuel and energy consumption analysis. His work also contributed to the European Commission's CO2MPAS Driver, a driving simulation software, and OpenACC, a database of automated vehicles' driving behavior. He has published more than 25 scientific papers in peer-reviewed journals and conference proceedings in automotive, transportation, and energy engineering.

Dr. He received prestige awards, including the 2020 Best Simulation Paper from the SimSub Committee of the Transportation Research Board (TRB) of the U.S. National Academy of Science, the 2021 Chinese Government Award for Outstanding Self-Financed Students Abroad, and the 2022 JRC Annual Award for Excellence in Research from the European Commission.

Konstantinos Mattas received the degree in civil engineering specialized in transportation, the M.Sc. degree in applied mathematics from the Democritus University of Thrace, Xanthi, Greece, and the Ph.D. degree from the Democritus University of Thrace, with a focus on fuzzy logic applications in transportation engineering. Since 2017, he has been with the Joint Research Centre, European Commission. His research interests include intelligent transportation systems, simulation of vehicle dynamics and driver behavior, microscopic simulation of traffic networks and network control, optimization, and traffic safety.

Michail A. Makridis (Member, IEEE) received the Ph.D. degree in computer vision from the Democritus University of Thrace, Greece. He is currently a Senior Research Scientist and the Deputy Director of the Traffic Engineering Group (SVT), ETH Zürich, Switzerland. Before, he was the scientific responsible for the Traffic Modeling Group of the Sustainable Transport Unit, Joint Research Centre (JRC), European Commission (EC). His research interests include traffic flow, management, and control for future intelligent transportation systems in the presence of connected and automated vehicles. In 2022, he received the JRC Annual Awards on Excellence in Research from the EC.

Dimitrios Komnos received the degree in mechanical engineering from the Aristotle University of Thessaloniki, Greece, in 2015, where he is pursuing the Ph.D. degree with a focus on the matter of vehicle energy consumption and emissions benchmarking under real-world operation. He is with European Joint Research Centre focusing on the EU policy for light duty vehicles CO2 emissions and energy consumption. His research interests include vehicle powertrains analysis, testing and simulation, CO2 certification, fleet analysis, and real-world fuel and energy consumption monitoring.

Andres L. Marín received the M.Sc. degree in data science with a specialization in deep learning. He is currently pursuing the Ph.D. degree with the Polytechnic University of Valencia with a focus on the machine learning design and deployment framework for energy-saving applications in the transport sector. He has a background in theoretical physics. Since 2020, he has been with the European Joint Research Centre, with a focus on data analysis for light duty vehicles' CO2 emissions and energy consumption. His research interests include machine learning, energy efficiency, and data analysis in the transport sector.

Georgios Fontaras received the Ph.D. degree from the Aristotle University of Thessaloniki. Since 2019, he has been a Visiting Associate Professor with the Department of Mechanical Engineering. He is currently a Researcher with the Joint Research Center, European Commission, leading the research project low energy and greenhouse emissions neutral transport. His activities focus on EU policy for road vehicle emissions abatement, vehicle and emissions simulation and inventorying, and scientific research for transport decarbonization. He is chairing the ERMES Informal Expert Group on emissions research and co-chairs the expert panel on transport of the UNECE task force for emissions inventories and projections. He has authored or coauthored more than 90 scientific publications in the area.

Biagio Ciuffo received the Ph.D. degree in transportation engineering from the Department of Transportation Engineering, University of Napoli Federico II, in 2008.

He held a three-year post-doctoral position with the Joint Research Centre (JRC), European Commission, Ispra, Italy, with a focus on the sustainability assessment of traffic and transport-related measures and policies. He is currently an Official of the European Commission, working for the Directorate for Energy, Mobility, and Climate, JRC. In the past, he has led different projects concerning the analysis of the environmental and economic impacts of different transport policies. He is also leading the JRC Project focusing on the wide implications of connected and automated mobility. He has published more than 120 scientific papers in peer-reviewed journals and conference proceedings in transportation and traffic engineering. He is also one of the main authors of the JRC Report on the Future of Road Transport, which analyzes the wide implications of connected, automated, low-carbon, and shared mobility.

Dr. Ciuffo has been awarded the 2012 Greenshields Prize from the Traffic Flow Theory and Characteristics Committee and the 2013 and 2020 Prizes of the SimSub Committee of the Transportation Research Board of the U.S. National Academy of Science, for his research activities on traffic simulation. He is the Deputy Editor-in-Chief of the *IET Intelligent Transport Systems* and an Associate Editor of IEEE TRANSACTIONS ON INTELLIGENT TRANSPORTATION SYSTEMS and serves as a reviewer for the most important journals in the transportation field.